Dalton Transactions

RSC Publishing

PAPER

View Article Online
View Journal | View Issue

Cite this: *Dalton Trans.*, 2013, **42**, 1385

Haloaurate and halopalladate imidazolium salts: structures, properties, and use as precursors for catalytic metal nanoparticles†

Christopher J. Serpell,‡[a] James Cookson,[b] Amber L. Thompson,[a] Christopher M. Brown[b] and Paul D. Beer*[a]

Received 29th August 2012,
Accepted 22nd October 2012

DOI: 10.1039/c2dt31984e

www.rsc.org/dalton

The synthesis and characterisation of a series of new gold- and palladium-containing symmetrical imidazolium salts are described which display significant cation-dependent effects determined by the structure of the alkyl chains of the imidazolium motifs. Whereas direct reduction of the Pd salts can produce stable nanoparticles (NPs) coated by imidazolium salts, the addition of strong base to the Pd or Au salts before reduction gives stable NPs, potentially pacified by *N*-heterocyclic carbene units. The possibility of NP surface protection by metal–carbon bonds in these systems is investigated by spectroscopic, synthetic, and catalytic investigations, providing support for the hypothesis. Significantly, the catalytic activity of the NPs is not inhibited by the continued presence of the ligands.

Ionic liquids (ILs) have been intensively studied as task-specific solvents.[1–4] Since the cation and anion can be varied at will (subject to effects upon the melting point), an enormous variety of solvents may be accessed with ease. Imidazolium salts in particular have risen to the fore due to their ease of synthesis. While most ILs designed as reaction media make use of inert, non-coordinating ions such as BF_4^- and PF_6^-, there is also substantial interest in the "added value" obtained using active species, such as metallate anions. Metal-containing ILs[5] in particular have been studied for a variety of motivations: primarily for catalysis,[6–9] but also metal deposition,[10] electrochemistry,[11] magnetism,[12] and photophysics.[13,14]

There is also considerable interest in the catalytic applications of metal nanoparticles (NPs) in imidazolium ionic liquids,[15–17] despite the fact that the nature of the interaction between the ionic liquid and metal NPs remains controversial. Early studies using XPS revealed interactions between the surface and the anions of the solvent (even weakly coordinating species). These results suggested that the anions form a coating over the surface (often positively charged), which is further surrounded by a layer of cations, thus providing stabilisation *via* the creation of Coulombic repulsions between NPs. This is known as the DLVO (Derjaguin–Landau–Verwey–Overbeek) model[18] (Fig. 1a). In 2005 Finke reported hydrogen-deuterium exchange at all aromatic positions of the 1-butyl-3-methylimidazolium cation catalysed by iridium NPs, and concluded that *N*-heterocyclic carbene (NHC)-type stabilisation

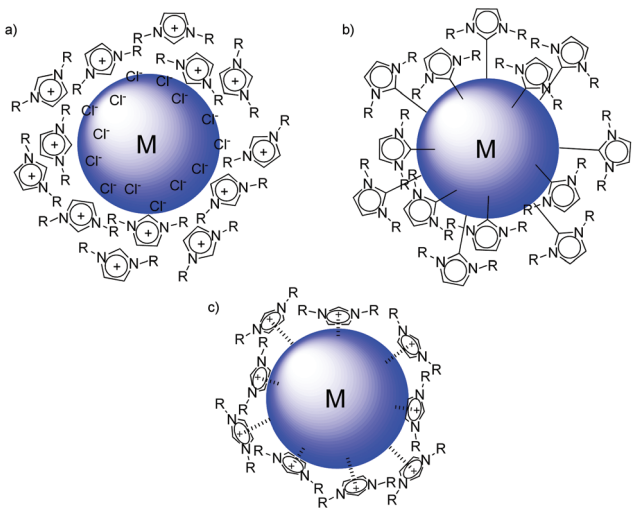

Fig. 1 Possible stabilisation modes for nanoparticles in ionic liquids.

[a]*Chemistry Research Laboratory, Department of Chemistry, University of Oxford, Mansfield Road, Oxford OX1 3TA, UK. E-mail: paul.beer@chem.ox.ac.uk; Fax: +44 (0)1865 272609; Tel: +44 (0)1865 285142*
[b]*Johnson Matthey Technology Centre, Blount's Court, Sonning Common, Reading, RG4 9NH, UK. E-mail: cooksj@matthey.com; Fax: +44 (0)118 924 2338; Tel: +44 (0)118 924 2061*

†Electronic supplementary information (ESI) available: Further TEM images, and crystal structures in .cif format. CCDC 898614–898618. For ESI and crystallographic data in CIF or other electronic format see DOI: 10.1039/c2dt31984e

‡Current address: Department of Chemistry, McGill University, Room 400, 801 Sherbrooke St. W., Montreal, Quebec, H3A 0B8, Canada, christopher.serpell@mcgill.ca

occurs, at least transiently (Fig. 1b).[19] However, in 2007, Dupont disclosed results of surface-enhanced Raman scattering (SERS) studies on Au NPs which indicated that surface stabilisation was occurring through parallel coordination by the imidazolium cation (Fig. 1c).[20] Even more recently, it has been claimed that the true stabilisers are actually methyl imidazole impurities present in the ionic liquid,[21] whereas on the other hand the direct synthesis of NHC-AuNPs has been reported from molecular NHC precursors[22] or *via* ligand displacement.[23] The actual situation may well depend on the exact system in question.

Herein we describe the synthesis and characterisation of a series of Au- and Pd-containing imidazolium salts and report a new preparative route to catalytically active NPs, *via* reduction of the metallate imidazolium ionic liquid.

Synthesis and characterisation of halometallate imidazolium salts

Bis(*N*,*N*′-propyl)imidazolium bromide (**2a**) and bis(*N*,*N*′-hexyl)-imidazolium bromide (**2b**) were prepared by sequential alkylation (Scheme 1). Imidazole, sodium hydride and alkyl bromides were used to give **1a** and **1b**; this was followed by refluxing in acetone with the same alkyl bromide, to afford room temperature ILs in good yields. Conversely, bis(*N*,*N*′-*tert*-butyl)imidazolium chloride (**2c**), a waxy solid, was synthesised *via* a three-component reaction,[24] due to the poor reactivity of the hindered *tert*-butyl bromide in the reactions described above. Biphasic anion exchange of these imidazolium halide salts **2a–c** using either $HAuCl_4$ or K_2PdCl_4 followed by solvent evaporation gave the metallic imidazolium salts (Scheme 1). In the case of the propyl species crystalline solids were obtained: **3a** was deep red (mp 96 °C), whereas **4a** was brown (mp 100 °C). Conversely, the di-hexyl salts manifested initially as liquids: blood red (**3b**) and deep brown (**4b**). In contrast to the first two chloroaurate salts, the bis(*tert*-butyl) analogue **3c** (crystalline solid, mp 132 °C) was bright yellow. The chloropalladate **4c** (crystalline solid, mp 204 °C) followed the trend of the other palladium salts, being deep brown.

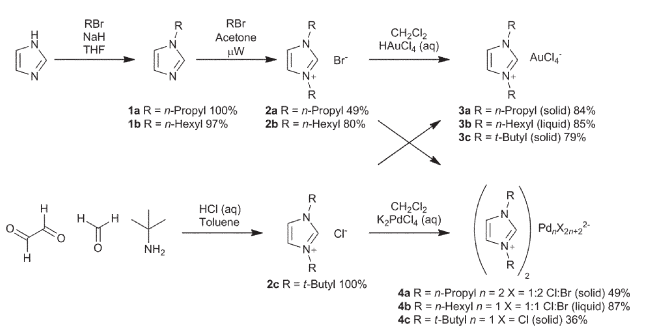

Scheme 1 Synthesis of chlorometallate imidazolium salts.

Crystals suitable for single crystal X-ray diffraction structural analysis§ of **3a**, **3c**, **4a**, and **4c** were obtained by slow evaporation of chloroform solutions. The bis(hexyl) salt, **4b**, was liquid but found to crystallise slowly over the course of two years and yielded small crystals which could be studied using synchrotron radiation.

The crystal structure of **3a** (Fig. 2) consists of alternating layers of anions and cations, primarily linked by anion–π interactions, but with some C–H···Cl hydrogen bonds. The two crystallographically independent imidazolium species are totally disordered, each requiring modelling over two sites. This lack of order in the solid state can be considered to be reciprocal to the higher order displayed by ionic liquids when compared to conventional solvents. The anion layers consist of $AuCl_4^-$ units in an edge-to-face arrangement, with the chloride of one approaching the metal atom of the next such that the $AuCl_4^-$ units are perpendicular. This arrangement has also been reported for similar systems.[25]

In **3c** (Fig. 3) the cations and anions are now located in an alternating array – a version of the sodium chloride structure with non-isotropic, mutually canted ions. Such an arrangement permits the optimisation of electrostatic forces, while also providing room for anion–π interactions. Although it could be suggested that this separation of the anions is responsible for the yellow colouration of the material, and the edge-to-face interaction in **3a** causes the red colour, previously reported $AuCl_4^-$ imidazolium systems have been documented to be yellow[11,25] or orange,[26] whether or not they contain this perpendicular arrangement of anions.

The motif of alternating layers of anions and cations seen in **3a** was repeated in the crystal structure of **4a** (Fig. 4), although it revealed not the expected tetrachloropalladate

§Single crystal diffraction data were collected using a Nonius Kappa CCD or using Beamline I19[32] at Diamond Light Source and processed with DENZO-SMN[33] or CrystalClear[34] including unit cell refinement and inter-frame scaling. Structures were solved with SHELXS,[35] SIR92[36] or SuperFlip[37] and refined using SHELXTL[35] or CRYSTALS[38–40] as per the SI (CIF). Crystallographic data (excluding structure factors) have been deposited with the Cambridge Crystallographic Data Centre (CCDC 898614–898618) and can be obtained *via* www.ccdc.cam.ac.uk/data _request/cif. Single crystal data **3a**: $C_9H_{17}AuCl_4N_2$, M_r = 492.01, 150 K, orthorhombic, *Pccn*, a = 19.7735(2), b = 9.3333(1), c = 17.0270(2) Å, V = 3142.37(6) Å^3, Data/restraints/parameters – 3539/54/99, R_{int} = 0.0242, R_1 = 0.0550, wR_2 = 0.1597 ($I > 2\sigma(I)$). **3c**: $C_{11}H_{21}AuCl_4N_2$, M_r = 520.08, 150 K, orthorhombic, *Cmc*2$_1$, a = 9.9772(2), b = 14.7125(3), c = 11.6742(3) Å, V = 1713.65(7) Å^3, Data/restraints/parameters – 1917/45/103, R_{int} = 0.060, R_1 = 0.0284, wR_2 = 0.0633 ($I > 2\sigma(I)$). **4a**: $C_{18}H_{34}Br_4Cl_2N_4Pd_2$, M_r = 909.83, 150 K, monoclinic, $P2_1/n$, a = 7.8505(3), b = 17.5620(6), c = 10.8085(4) Å, β = 94.616(2)°, V = 1485.34(9) Å^3, Data/restraints/parameters – 3358/0/144, R_{int} = 0.0863, R_1 = 0.0438, wR_2 = 0.0772 ($I > 2\sigma(I)$). **4b**: $C_{30}H_{58}Br_{1.78}Cl_{2.22}N_4Pd$, M_r = 802.16, 100 K, triclinic, $P\bar{1}$, a = 7.682(4), b = 9.105(6), c = 13.838(10) Å, α = 82.14(2)°, β = 78.97(2)°, γ = 68.59(2)°, V = 882.1(10) Å^3, Data/restraints/parameters – 5425/0/186, R_{int} = 0.029, R_1 = 0.0414, wR_2 = 0.0675 ($I > 2\sigma(I)$). These data were collected using synchrotron data and the sample suffered radiation damage. Since the crystals took two years to grow, the experiment could not easily be repeated; although the data are incomplete, it is not expected to have a significant influence on the structure determination. **4c**: $C_{22}H_{42}Cl_4N_4Pd$, M_r = 610.81, 150 K, monoclinic, *C*2/*m*, a = 17.3545(7), b = 9.4171(5), c = 10.5259(5) Å, β = 125.898(2)°, V = 1393.50(12) Å^3, Data/restraints/parameters – 1673/0/91, R_{int} = 0.031, R_1 = 0.0344, wR_2 = 0.0769 ($I > 2\sigma(I)$).

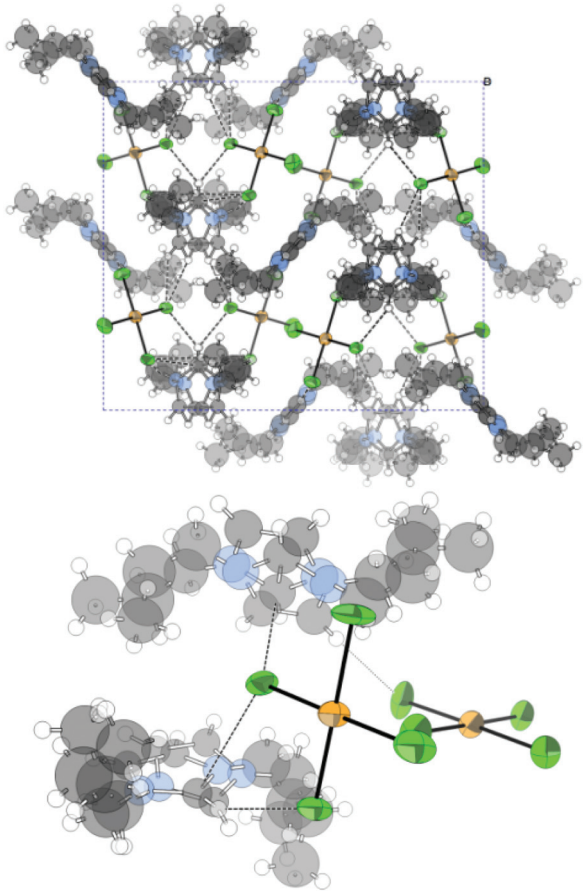

Fig. 2 Two views of the crystal structure of **3a**; showing packing in layers of cations and anions (top), and detail of disorder, and interactions between the ions (bottom). Thermal ellipsoids displayed at 50% probability.

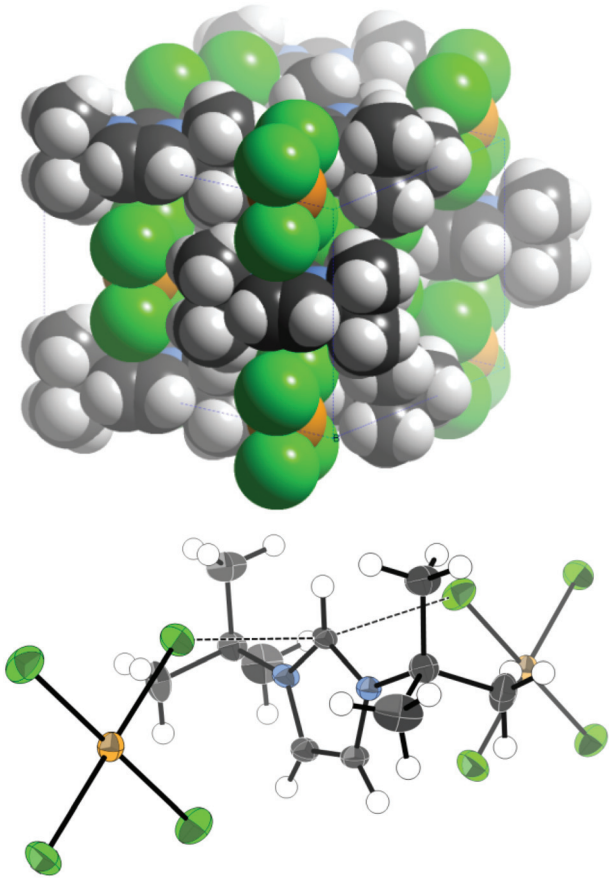

Fig. 3 Two views of the crystal structure of **3c**; showing pseudo-NaCl structure packing in space-filling representation (top), and detail of anion–π interactions (bottom). Thermal ellipsoids displayed at 50% probability.

dianion, but a dinuclear bromide bridged Pd(II) species, terminated with halides (chlorides and bromides occurring in a 50 : 50 ratio). The formation of this anion must have occurred during the anion exchange process in which the labile tetrachloropalladate would have encountered aqueous bromide anions. The Pd : Br ratio of 1 : 2 in the anion exchange reaction mixture is preserved here, suggesting that the structure is indeed representative of the bulk sample, rather than being an example of selective crystallisation effects. Using mass spectrometry to demonstrate whether these dimeric species were the only ones present before crystallisation was inconclusive.

The same partial halide exchange process also occurred for the hexyl analogue, **4b** (Fig. 5). Interestingly, although this substitution was seen in this work when attempting $Br^-/PdCl_4^{2-}$ exchange, it did not occur with $AuCl_4^-$, despite having been observed by others.[27] In the case of **4b** the metal anion remained monomeric, which is surprising given that large cations are known to promote dimerisation.[28] A possible explanation comes from the prevalence of hydrogen bonding in this structure over anion–π interactions, which are complemented by a more concentrated negative charge. Interestingly, in this case weak chelating hydrogen bonds were observed between the protons in the 4- and 5-positions on the imidazolium ring and one of the halides, an effect that has been previously discussed,[29,30] but rarely observed directly.

The crystal structure of **4c** (Fig. 6) also featured anion–π interactions as a packing motif. That these occur significantly in both of the *tert*-butyl imidazolium salts is probably due to steric hindrance of the acidic protons. In this structure the $PdCl_4^{2-}$ anion is observed, without dimerisation, which is typical for crystals with more compact cations.

Synthesis of nanoparticles *via* reduction of metallate ionic liquids

Having prepared the imidazolium metallate precursors, reductions were performed with the aim of producing imidazolium and/or carbene stabilised nanoparticulate Au and Pd materials (Scheme 2).

Firstly, direct borohydride reduction of the bis(hexyl) imidazolium metallate salts **3b** and **4b** was conducted in 1 : 1 dichloromethane–toluene in an ice bath. In the case of the Pd salt **4b** this gave stable black NPs **5b**, whereas using **3b** to obtain **5a** gave only agglomerated bulk metal. To ensure that the stability of the Pd NPs compared with the Au system was not due to the extra equivalent of stabiliser in the former case,

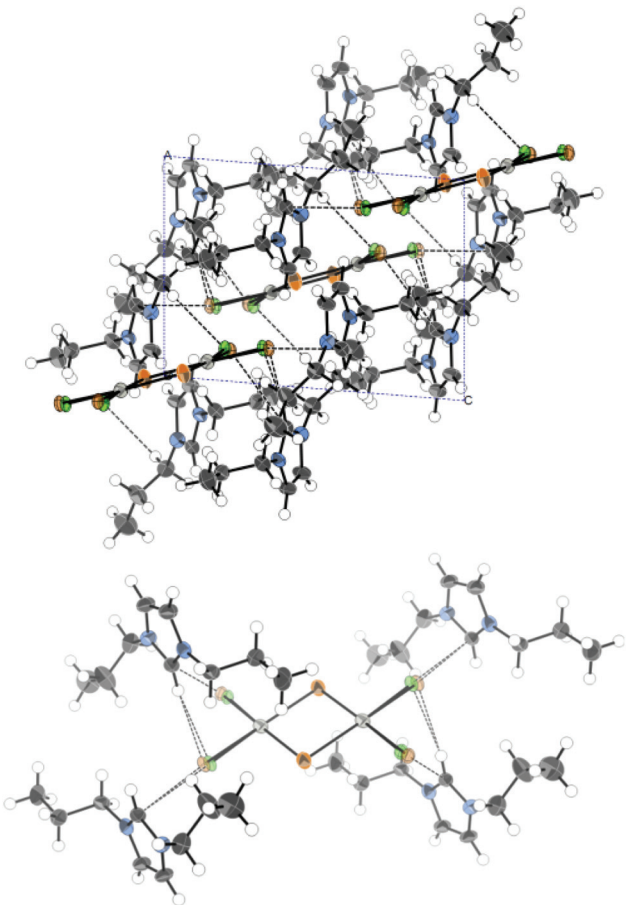

Fig. 4 Two views of the crystal structure of **4a**; showing packing in layers of cations and anions (top), and detail of disorder, H-bonding and anion–π interactions (bottom). Thermal ellipsoids displayed at 50% probability.

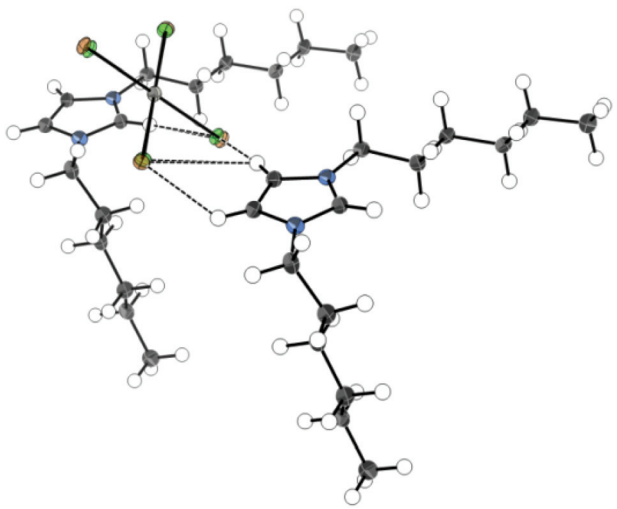

Fig. 5 Crystal structure of **4b**. Thermal ellipsoids displayed at 50% probability.

the Au reduction was attempted again in the presence of one equivalent of bis(*N*,*N*′-hexyl)imidazolium chloride, but no stable NPs were formed.

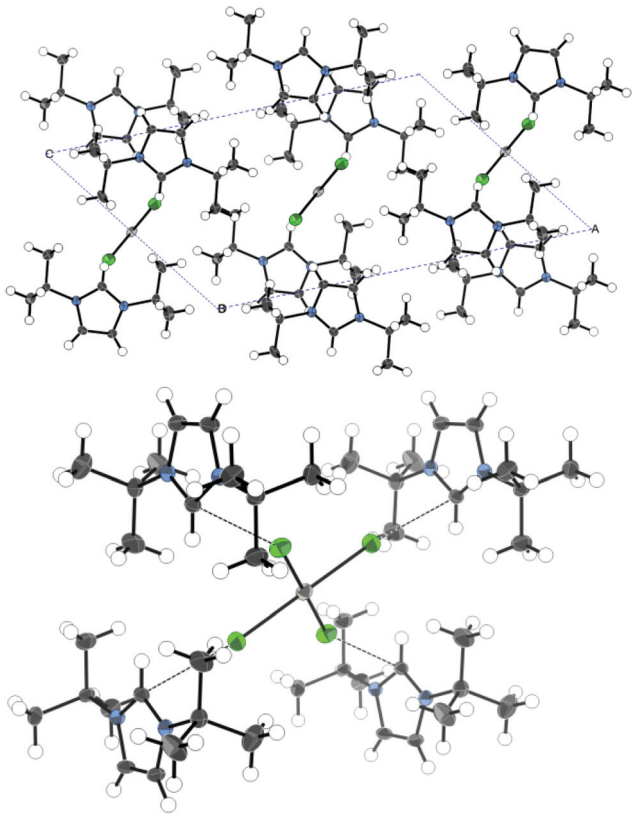

Fig. 6 Two views of the crystal structure of **4c**; showing packing in layers (top), and detail of anion–π interactions (bottom). Thermal ellipsoids displayed at 50% probability.

Attempts were then made to promote NHC-stabilisation of NPs by deprotonation of the imidazolium cation prior to reduction. This was achieved by treating the imidazolium salt with sodium hydride in 1 : 1 dichloromethane–toluene, before adding sodium borohydride to reduce the metals. This generated stable Au and Pd NPs **6a** and **6b** respectively as purple and black solutions.

UV-vis spectroscopy of Au NPs **6a** revealed a strong plasmon resonance band at 514 nm, while as expected none was observed for the Pd NPs. Examination of the ^{1}H NMR spectrum of **6a** in $CDCl_3$ (Fig. 7) revealed the disappearance of the acidic imidazolium C2 proton resonance (*a*), while broadening and splitting was observed for the other peaks (*b*–*h*), typical of NP-coordinated ligands. ^{13}C NMR also failed to locate a peak for C2, which is thought to be due to anisotropy resulting from the surface coordination. Conversely, for the Pd NPs produced without deprotonation (**5b**) the C2 ^{1}H peak was observed at 8.10 ppm.

TEM analysis of the three samples (Fig. 8) showed that the Pd NPs were small and monodisperse with sizes of 1.8 nm (±0.4, n = 261) and 2.7 nm (±0.9, n = 191) for **5b** and **6b** respectively. The Au NPs **6a** were significantly larger and more polydisperse at 16.6 nm (±6.5, n = 133), a fact which points towards a weaker stabilisation of the Au surface by the NHC ligands compared to Pd. Indeed, the NHC capping of Pd NPs (**7**) also resulted in greater NP diameters than was seen for apparent

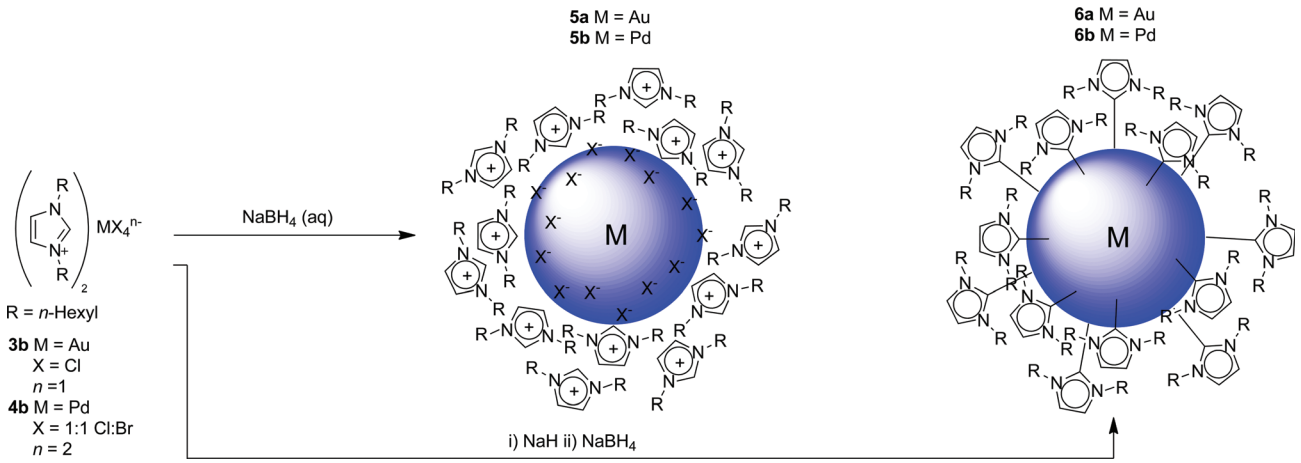

Scheme 2 Synthesis of imidazolium and NHC stabilised NPs.

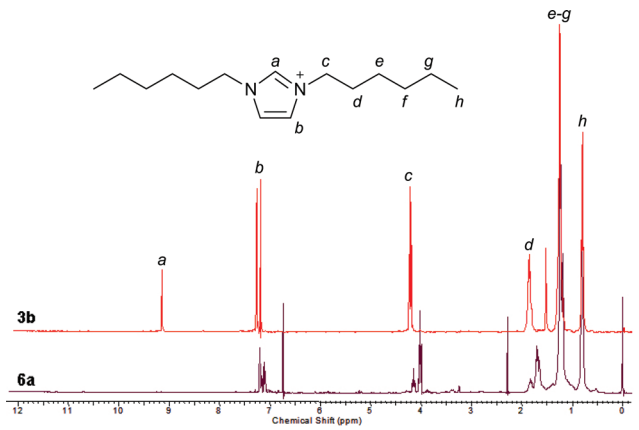

Fig. 7 ^{1}H NMR spectra of ionic liquid **3b** and Au NPs **6a** ($CDCl_3$, 293 K).

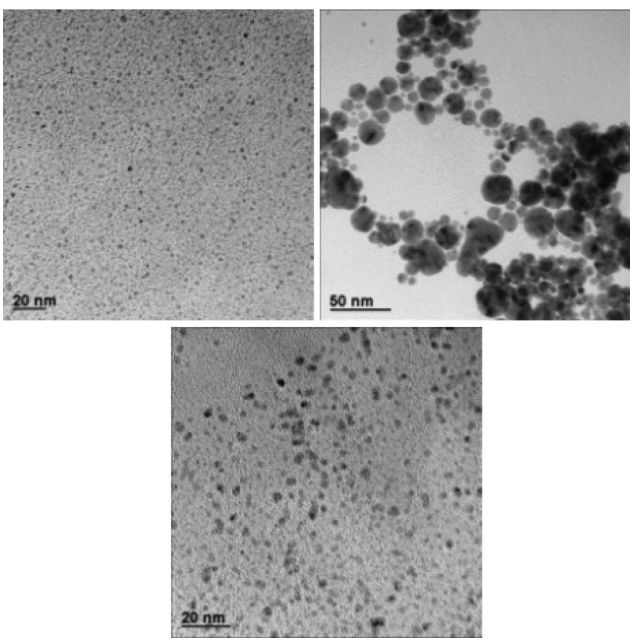

Fig. 8 TEM images of **5b** (left), **6a** (right), and **6b** (bottom).

surfactant stabilisation (**5b**) suggesting again that while the NPs were sufficiently stable to characterise, NHCs are comparatively poor pacifying agents for metal NPs.

These results are consistent with the NHC coordination mode in **6a** and **6b**. The implication of this type of capping ligands is reaffirmed by the fact that stable Au NPs could *only* be generated when the imidazolium cation was deprotonated, permitting coordination of the surface through M–C bonds.

Using the bis(propyl) or bis(*tert*-butyl) chlorometallate imidazolium salts in either of these protocols failed to give stable NPs. In the former case, this is probably due to the propyl chains being insufficiently bulky to prevent close approach and subsequent thermodynamically favourable coagulation of NPs, whereas for the latter example, it could also be due to additional methyl groups sterically preventing the formation of strong C–M bonds to surfaces.

Catalytic studies with palladium nanoparticles

In order to test the catalytic activity of the NP samples, and in particular test the differences due to coordination mode, portions of the Pd NPs **5b** and **6b** were adsorbed onto activated carbon (Norit GSX) to give a 2.5 wt% loading with respect to the metal. These samples were then characterised by ICP-ES and TEM, confirming the level of metal present and checking for any changes in structure due to the support. TEM analysis of the samples on carbon gave new NP diameters – it was found that the surfactant stabilised Pd NPs **5b** had increased in average diameter from 1.8 nm to 3.5 nm (±1.4, n = 110), while the NHC Pd NPs **6b** remained almost exactly the same at 2.6 nm (±1.2, n = 99). This suggests that the more well-defined, bonded coordination of **6b** promotes NP stability and rigidity, while the fluid surfactant stabilisation permits partial agglomeration.

In these cases the presence or absence of ligand could prove vital – while surfactant stabilisation is not expected to block the NP surface to catalytic substrates, a strong M–C NHC bond could well impede activity. Portions of the samples were therefore calcined in air at 450 °C to remove the ligands

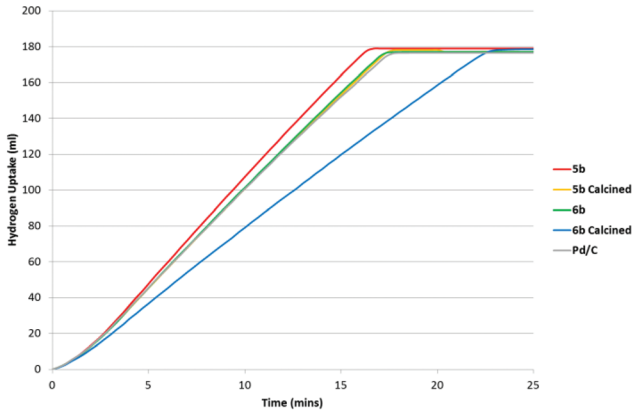

Fig. 9 Hydrogen uptake curves for the reduction of nitrobenzene to aniline catalysed by Pd NPs **5b** and **6b**. Reaction conditions: 3 bar H_2, 50 °C, 1 : 1000 catalyst to substrate molar ratio.

Table 1 Rates of hydrogen uptake in the reduction of nitrobenzene to aniline catalysed by Pd NPs **5b** and **6b**[a]

Catalyst	Reaction rate (ml min^{-1})
5b	11.7
5b (calcined)	10.9
6b	11.0
6b (calcined)	8.3
Pd/C standard	10.7

[a] Reaction conditions: 3 bar H_2, 50 °C, 1 : 1000 catalyst to substrate molar ratio, ±5% estimated error.

(the optimal temperature was determined by thermogravimetric analysis). The reduction of nitrobenzene to aniline was then performed using the prepared catalysts.

The tests revealed complete conversion of nitrobenzene to aniline within half an hour by all the samples, as well as by a commercial Pd/C standard (Fig. 9). The differences in the reaction rates (Table 1) and hence catalytic potency of the samples – which cannot be correlated with NP surface area – can be used to derive information about the physicochemical environment at the catalytic sites. The imidazolium-protected NPs **5b** were the most active, which is in concord with the expected fluidity of the ionic liquid coating permitting access of the substrate to the catalytic surface. The carbene-protected NPs **6b** were less active (on a par with the Pd/C standard), which implies a slightly less accessible surface, though still retaining a useful level of potency. This is consistent with the formation of a stronger bond between the surface and the ligand. For both **5b** and **6b** calcination to remove the ligands resulted in a decrease in reaction rate, which is likely to be due to some degree of sintering and particle growth, but more significantly indicates that the imidazolium moieties do not inhibit the catalytic activity of the nanoparticles in either protecting mode, and may indeed promote it. We have previously demonstrated the advantages of functional supramolecular ligands for the formation of catalytically optimised metal NPs,[31] and the retained activity of the NPs discussed herein suggest that further novel systems could be produced through judicious (and synthetically facile) modifications of the imidazolium side-chains.

Conclusions

We have reported the synthesis of a series of new gold- and palladium-containing imidazolium salts, and obtained crystal structures for those solid at room temperature. These structures reveal a broad spectrum of interactions which are highly dependent upon the structure of the alkyl chains of the imidazolium motifs. The stability of Au and Pd NPs produced by reduction of these species is also determined by the nature of the alkyl side chains, as well as the metal, and the presence or absence of base, giving surfactant or NHC stabilised NPs. Importantly the Pd samples retain their catalytic activity for the reduction of nitrobenzene to aniline despite the continued presence of the ligands on the surface, a significant finding for the future production of novel task-specific catalysts.

Experimental

Instrumentation

NMR spectra were recorded on a Varian Mercury VX300, Varian Unity Plus 500, Bruker DPX200, or Bruker AVC500 spectrometer. All ^{13}C spectra were proton decoupled. Mass spectrometry was performed on a Bruker microTOF (ESI) or a Waters Micromass MALDI micro MX (MALDI-TOF) mass spectrometer. Melting points were recorded on a Gallenkamp capillary melting point apparatus and are uncorrected. Microwave reactions were carried out using a Biotage Initiator 2.0 microwave. UV-vis spectra were recorded on a PG Instruments T60U spectrometer or Shimadzu UV-2401PC UV-Vis photospectrometer. Samples were prepared in a 3 ml quartz cuvette and concentrations were adjusted to suit the absorption range of the instrument. Thermogravimetric analysis was performed using a PerkinElmer Diamond TG/DTA. Calcination was performed using a Carbolite RHF 1600 furnace. ICP-ES analyses were undertaken using a PerkinElmer Optima 3300RL instrument. Samples were prepared by Na_2O_2 infusion in a zirconium crucible and compared against standard gravimetrically determined solutions. TEM was conducted using a Tecnai F20 Transmission Electron Microscope with a voltage of 200 kV, and C2 aperture of 30 and 50 m, in bright field (BF) and STEM (HAADF) mode, and performing *in situ* EDX analysis. A small portion of the sample was crushed and then dusted onto a holey carbon film on a TEM grid (Cu). Approximately 12 micrographs were recorded for each sample.

Synthesis

Commercially available materials were used without any pretreatment unless otherwise stated. Dry solvents were obtained by purging with N_2 and then passing through an MBraun MPSP-800 column. H_2O was de-ionised and microfiltered using a Milli-Q® Millipore machine.

1-Propyl-1*H*-imidazole (1a). Sodium hydride (60% dispersion in mineral oil, 0.15 g, 3.8 mmol) was suspended in 10 ml dry THF under nitrogen at 0 °C. Imidazole (0.25 g, 3.67 mmol) was dissolved in 5 ml dry THF and added dropwise. After gas evolution stopped, 1-bromopropane (0.44 g, 3.67 mmol) in 5 ml dry THF was also added dropwise. The resultant mixture was then stirred at room temperature overnight. After careful addition of a few drops of water to quench the hydride, the organic solvent was removed and diethyl ether (25 ml) was added. This solution was washed three times with water (25 ml), and the combined aqueous layers were re-extracted with diethyl ether (50 ml). The collected organic layers were then dried over $MgSO_4$ and filtered. Solvent removal gave **1a** as a pale yellow oil (0.40 g, 100%). ^{1}H NMR (300 MHz, $CDCl_3$) δ (ppm) 7.45 (1H, s, Im*H*), 7.04 (1H, s, Im*H*), 6.89 (1H, s, Im*H*), 3.88 (2H, t, ^3J = 7.0 Hz, CH_2), 1.79 (2H, tq, ^3J = 7.0, 7.3 Hz, CH_2), 0.91 (3H, t, ^3J = 7.3 Hz, CH_3); ESMS: *m*/*z* calc. for $[M + H]^+$ 111.09, found 111.09.

1-Hexyl-1*H*-imidazole (1b). Prepared as for **1b** using sodium hydride (60% dispersion in mineral oil, 3.15 g, 78.8 mmol), imidazole (4.47 g, 65.7 mmol) and 1-bromohexane (10.85 g, 65.7 mmol) giving the product as a yellow oil (9.74 g, 97%). ^{1}H NMR (300 MHz, $CDCl_3$) δ (ppm) 7.47 (1H, s, Im*H*), 7.06 (1H, s, Im*H*), 6.91 (1H, s, Imr*H*), 3.93 (2H, t, ^3J = 7.2 Hz, NCH_2), 1.77, (2H, m, NCH$_2$CH_2), 1.29 (6H, m, –(CH_2)$_3$–), 0.88 (6H, t, ^3J = 6.7 Hz, CH$_2$CH_3); ESMS: *m*/*z* calc. for $[M + H]^+$ 153.13, found 153.12.

1,3-Dipropyl-1*H*-imidazol-3-ium bromide (2a). **1a** (2.00 g, 18 mmol) and 1-bromopropane (5.50 g, 45 mmol) were refluxed in acetone (250 ml) overnight. The solvent was removed, and the resultant oil was washed with diethyl ether (3 × 25 ml) to extract any starting materials, leaving **2a** as a pure yellow oil (2.07 g, 49%). ^{1}H NMR (300 MHz, $CDCl_3$) δ (ppm) 10.74 (1H, s, Im*H*), 7.32 (2H, s, Im*H*), 4.35 (4H, t, ^3J = 7.4 Hz, CH_2), 1.99 (4H, tq, ^3J = 7.3, 7.4 Hz, CH_2), 1.00 (6H, t, ^3J = 7.4 Hz, CH_3); ESMS: *m*/*z* calc. for $[M - Br]^+$ 153.13, found 153.10.

1,3-Dihexyl-1*H*-imidazol-3-ium bromide (2b). **1b** (0.34 g, 1.88 mmol) and 1-bromohexane (0.37 g, 2.26 mmol) were heated to 150 °C in 3 ml acetone in a sealed vial under microwave irradiation for ten minutes. The solvent was removed and the resultant oil stirred extracted with diethyl ether (3 × 20 ml) to remove excess 1-bromohexane. The remaining yellow oil constituted the pure bromide salt (0.50 g, 80%). ^{1}H NMR (300 MHz, $CDCl_3$) δ (ppm) 10.36 (1H, s, Im*H*), 7.45 (2H, s, Im*H*), 4.27 (4H, t, ^3J = 7.6 Hz, NCH_2), 1.83, 4H, m, NCH$_2$CH_2), 1.22 (12H, m, –(CH_2)$_3$–), 0.77 (6H, t, ^3J = 6.5 Hz, CH$_2$CH_3); ^{13}C NMR (75 MHz, $CDCl_3$) δ 137.0, 121.9, 49.8, 30.9, 25.6, 22.2, 13.7; ESMS: *m*/*z* calc. for $[M - Br]^+$ 237.23, found 237.21.

1,3-Di-*tert*-butyl-1*H*-imidazol-3-ium chloride (2c).[24] Paraformaldehyde (1.00 g, 3.33 mmol) was suspended in toluene (20 ml), and *tert*-butylamine (2.44 g, 3.33 mmol) was added dropwise. The mixture was then heated with stirring until a clear solution was obtained. The solution was cooled in an ice bath, and further *tert*-butylamine (2.44 g, 3.33 mmol) was added dropwise, followed by conc. HCl (aq) (3.28 ml, 3.33 mmol), and then glyoxal (40% aq, 4.83 ml, 3.33 mmol). The reaction mixture was heated to 40 °C for 15 hours, after which the organic solvent was removed *in vacuo*. The resulting aqueous mixture was extracted with CH_2Cl_2 (2 × 20 ml) to remove side products. The water was evaporated under vacuum and the solid was extracted by trituration with CH_2Cl_2 (3 × 50 ml), giving **2c** as an off-white solid after solvent removal (4.44 g, 100%). ^{1}H NMR (300 MHz, $CDCl_3$) δ (ppm) 10.65 (1H, s, Im*H*), 7.37 (2H, s, Im*H*), 1.81 (18H, s, CH_3); ESMS: *m*/*z* calc. for $[M - Cl]^+$ 181.1, found 181.1.

1,3-Dipropyl-1*H*-imidazol-3-ium tetrachloroaurate (3a). **2a** (0.10 g, 0.42 mmol) was dissolved in $CHCl_3$ (12 ml) and stirred vigorously with $HAuCl_4$ (0.15 g, 0.42 mmol) dissolved in water (12 ml). After approximately two hours the yellow colouration of the aqueous layer had disappeared, to be replaced by a deep red colour in organic portion. The solvent was removed from the organic layer, giving **3a** as an orange-red crystalline solid (0.12 g, 84%). ^{1}H NMR (300 MHz, acetone-d$_6$) δ (ppm) 9.16 (1H, s, Im*H*), 7.84 (2H, s, Im*H*), 4.37 (4H, t, ^3J = 7.2 Hz, CH_2), 1.99 (4H, tq, ^3J = 7.2, 7.3 Hz, CH_2), 0.97 (6H, t, ^3J = 7.3 Hz, CH_3); ^{13}C NMR (125 MHz, 10 : 1 $CDCl_3$–CD_3OD) δ 135.5, 123.1, 52.4, 24.0, 11.2; HR-ESMS: *m*/*z* calc. for $[M - AuCl_4]^+$ 153.1392, found 153.1390; ESMS: *m*/*z* calc. for $[M - Pr_2Im]^-$ 336.84, found 336.82; mp 96 °C.

1,3-Dihexyl-1*H*-imidazol-3-ium tetrachloroaurate (3b). As for **3a**, using **2b** (0.15 g, 0.47 mmol) and $HAuCl_4$ (0.16 g, 0.47 mmol), giving **3b** as a blood red oil (0.23 g, 85%). ^{1}H NMR (300 MHz, $CDCl_3$) δ (ppm) 9.22 (1H, s, Im*H*), 7.35 (2H, s, Im*H*), 4.30 (4H, t, ^3J = 7.5 Hz, CH_2), 1.95 (4H, m, CH_2), 1.36 (12H, m, CH_2) 0.90 (6H, t, ^3J = 7.0 Hz, CH_3); ^{13}C NMR (75 MHz, $CDCl_3$) δ 134.9, 122.5, 50.7, 31.0, 30.1, 25.9, 22.4, 13.9; ESMS: *m*/*z* calc. for $[M - AuCl_4]^+$ 237.23, found 237.22, calc. for $[M - Hex_2Im]^-$ 338.84, found 338.85.

1,3-Di-*tert*-butyl-1*H*-imidazol-3-ium tetrachloroaurate (3c). chloride **2c** (0.50 g, 2.3 mmol) was dissolved in $CHCl_3$ (25 ml) and $HAuCl_4$ (0.78 g, 2.3 mmol) dissolved in water (25 ml) was added, forming an emulsion. Both solvents were removed *in vacuo*, and the solid was extracted by trituration with CH_2Cl_2 (3 × 50 ml). Evaporation of the combined organic phases gave **3c** as a yellow crystalline solid (0.95 g, 79%). ^{1}H NMR (300 MHz, $CDCl_3$) δ (ppm) 9.23 (1H, s, Im*H*), 7.46 (2H, s, Im*H*), 1.79 (18H, s, CH_3); ^{13}C NMR (125 MHz, 9 : 1 $CDCl_3$–CD_3OD) δ 130.7, 120.1, 60.4, 29.5; ESMS: *m*/*z* calc. for $[M - AuCl_4]^+$ 181.1, found 181.1; mp 132 °C.

1,3-Dipropyl-1*H*-imidazol-3-ium halopalladate (4a). **2a** (0.20 g, 0.84 mmol) was dissolved in $CHCl_3$ (12 ml) and stirred vigorously with K_2PdCl_4 (0.13 g, 0.42 mmol) dissolved in water (12 ml). After four hours the colour had transferred from the aqueous layer to the organic portion, although some oiling out was observed, which was countered by addition of CH_2Cl_2 (5 ml). The layers were separated, and solvent removed from the organic fraction, giving **4a** as a dark brown crystalline solid (0.22 g, 49%). ^{1}H NMR (300 MHz, CD_3OD) δ (ppm) 9.21 (1H, s, Im*H*), 7.77 (2H, s, Im*H*), 4.34 (4H, t, ^3J = 7.2 Hz, CH_2), 2.02 (4H, tq, ^3J = 7.2, 7.3 Hz, CH_2), 1.02 (6H, t, ^3J = 7.3 Hz, CH_3); ^{13}C NMR (75 MHz, CD_3OD_3) δ 128.3, 124.1, 52.8, 25.2,

11.2; ESMS: *m*/*z* calc. for $[M - Pd_nX_m]^+$ 153.13, found 153.10; mp 100 °C.

1,3-Dihexyl-1*H*-imidazol-3-ium tetrahalopalladate (4b). As for **3a** using **2b** (0.70 g, 2.2 mmol) and K_2PdCl_4 (0.32 g, 1.1 mmol) giving **4b** as a deep brown oil, which crystallised over the course of two years (0.62 g, 87%). ^{1}H NMR (300 MHz, $CDCl_3$) δ (ppm) 10.08 (1H, s, Im*H*), 7.42 (2H, s, Im*H*), 4.55 (4H, t, ^3J = 7.5 Hz, CH_2), 1.98 (4H, m, CH_2), 1.32 (12H, m, CH_2) 0.87 (6H, t, ^3J = 7.2 Hz, CH_3); ^{13}C NMR (75 MHz, $CDCl_3$) δ 136.8, 122.1, 50.7, 31.1, 30.3, 26.0, 22.4, 14.0; ESMS: *m*/*z* calc. for $[M - Pd_nX_m]^+$ 237.23, found 237.22; mp 34 °C.

1,3-Di-*tert*-butyl-1*H*-imidazol-3-ium tetrachloropalladate (4c). 1,3-Di-*tert*-butyl-1*H*-imidazol-3-ium chloride **2c** (1.00 g, 4.6 mmol) and K_2PdCl_4 (0.75 g, 2.3 mmol) were stirred for two hours in water (50 ml). The water was removed *in vacuo*, and CH_2Cl_2 (50 ml) was used to dissolve the residue, which was then filtered through Celite. Rotary evaporation of the solvent gave **4c** as a dark brown crystalline solid (1.00 g, 36%). ^{1}H NMR (300 MHz, $CDCl_3$) δ (ppm) 9.84 (1H, s, Im*H*), 7.51 (2H, s, Im*H*), 1.81 (18H, s, CH_3); ^{13}C NMR (125 MHz, 9 : 1 $CDCl_3$–CD_3OD) δ 131.4, 120.2, 60.2, 29.4; ESMS: *m*/*z* calc. for $[M - PdCl_4]^+$ 181.1, found 181.1; mp 204 °C.

Pd NPs 5a. Bis-hexylimidazolium halopalladate **4b** (0.84 g, 1.16 mmol) was dissolved in 1 : 1 dry CH_2Cl_2–toluene (50 ml), and cooled in an ice bath. $NaBH_4$ (0.22 g, 5.80 mmol) in water (5 ml) was added dropwise, with vigorous stirring, and the solution was further stirred at room temperature for two hours. The reaction mixture was washed with water (3 × 25 ml), filtered and the solvent removed *in vacuo* giving a brown-black oil (0.51 g). TEM mean diameter 1.8 nm (±0.4, *n* = 261).

Au NPs 6a. Sodium hydride (60% dispersion in mineral oil, 0.041 g, 1.04 mmol) was suspended in 1 : 1 dry CH_2Cl_2–toluene (40 ml) cooled in an ice bath. Bis-hexylimidazolium tetrachloroaurate **3b** (0.40 g, 0.69 mmol) dissolved in dry CH_2Cl_2 (10 ml) was added dropwise, and the reaction mixture was stirred for 20 min, exhibiting a colour change from red to yellow. $NaBH_4$ (0.13 g, 3.47 mmol) in water (5 ml) was administered dropwise, maintaining the temperature of the reaction using the ice bath. The reaction was stirred at room temperature for two hours, after which it was washed with water (3 × 50 ml), the aqueous portions being discarded. After filtration, rotary evaporation gave a **6a** as dark purple oil (0.21 g). UV-vis (toluene) PRB 514 nm; TEM mean diameter 16.6 nm (±6.5, *n* = 133).

Pd NPs 6b. The reaction was performed in the same manner as the preparation of **6a**, using NaH (60% dispersion in mineral oil, 0.12 g, 2.90 mmol), **4b** (0.70 g, 0.97 mmol), and $NaBH_4$ (0.18 g, 4.84 mmol), giving a black oil (0.35 g). TEM mean diameter 2.7 nm (±0.9, *n* = 191).

Catalytic tests

Catalytic hydrogenations were performed in a HEL ChemSCAN reactor. Within each reaction cell 5.0 ml of a 0.5 mol dm^{-3} solution of the substrate in ethanol with 1,4-dioxane (internal standard for GC) was used. The carbon-supported catalyst was added in the ratio 1 : 1000 molar ratio of Pd to substrate, making use of the ICP-ES data for bulk composition. The reactions were run at 50 °C under 3 bar of H_2. The composition of the organic phase was analysed by gas chromatography using a PerkinElmer Autosample XL Gas chromatograph fitted with a 30 m PE-5MS column. Quantification was achieved by comparison to known standard solutions. The GC was connected to a PerkinElmer TurboMass mass spectrometer to allow for determination of unknown peaks.

Acknowledgements

C. J. S. thanks the EPSRC and Johnson Matthey for a CASE studentship and the EPSRC for a PhD+ award. We are grateful to Diamond Light Source for the award of beamtime on I19 (MT1858) and to the beamline scientists for help and support.

Notes and references

1 J. Dupont, *Acc. Chem. Res.*, 2011, **44**, 1223–1231.
2 R. Giernoth, *Angew. Chem., Int. Ed.*, 2010, **49**, 2834–2839.
3 D. Freudenmann, S. Wolf, M. Wolff and C. Feldmann, *Angew. Chem., Int. Ed.*, 2011, **50**, 11050–11060.
4 S. Tang, G. A. Baker and H. Zhao, *Chem. Soc. Rev.*, 2012, **41**, 4030–4066.
5 I. J. B. Lin and C. S. Vasam, *J. Organomet. Chem.*, 2005, **690**, 3498–3512.
6 K. Bica and P. Gaertner, *Eur. J. Org. Chem.*, 2008, **2008**, 3453–3456.
7 J. E. L. Dullius, P. A. Z. Suarez, S. Einloft, R. F. de Souza, J. Dupont, J. Fischer and A. De Cian, *Organometallics*, 1998, **17**, 815–819.
8 M. H. Valkenberg, C. deCastro and W. F. Hölderich, *Appl. Catal., A*, 2001, **215**, 185–190.
9 J. E. Dengler, A. Doroodian and B. Rieger, *J. Organomet. Chem.*, 2011, **696**, 3831–3835.
10 N. R. Brooks, S. Schaltin, K. Van Hecke, L. Van Meervelt, K. Binnemans and J. Fransaer, *Chem.–Eur. J.*, 2011, **17**, 5054–5059.
11 B. Ballarin, L. Busetto, M. Cristina Cassani and C. Femoni, *Inorg. Chim. Acta*, 2010, **363**, 2055–2064.
12 S. Hayashi, S. Saha and H. Hamaguchi, *Magn. IEEE Trans.*, 2006, **42**, 12–14.
13 P. Nockemann, B. Thijs, N. Postelmans, K. Van Hecke, L. Van Meervelt and K. Binnemans, *J. Am. Chem. Soc.*, 2006, **128**, 13658–13659.
14 Y. Yoshida, J. Fujii, G. Saito, T. Hiramatsu and N. Sato, *J. Mater. Chem.*, 2006, 16.
15 P. Migowski and J. Dupont, *Chem.–Eur. J.*, 2007, **13**, 32–39.
16 C. W. Scheeren, G. Machado, J. Dupont, P. F. P. Fichtner and S. r. R. Texeira, *Inorg. Chem.*, 2003, **42**, 4738–4742.
17 J. Huang, T. Jiang, B. Han, H. Gao, Y. Chang, G. Zhao and W. Wu, *Chem. Commun.*, 2003, 1654–1655.
18 S. Ãzkar and R. G. Finke, *J. Am. Chem. Soc.*, 2002, **124**, 5796–5810.

19 L. S. Ott, M. L. Cline, M. Deetlefs, K. R. Seddon and R. G. Finke, *J. Am. Chem. Soc.*, 2005, **127**, 5758–5759.
20 H. S. Schrekker, M. A. Gelesky, M. P. Stracke, C. M. L. Schrekker, G. Machado, S. R. Teixeira, J. C. Rubim and J. Dupont, *J. Colloid Interface Sci.*, 2007, **316**, 189–195.
21 P. Dash and R. W. J. Scott, *Chem. Commun.*, 2009, 812–814.
22 J. Vignolle and T. D. Tilley, *Chem. Commun.*, 2009.
23 E. C. Hurst, K. Wilson, I. J. S. Fairlamb and V. Chechik, *New J. Chem.*, 2009, **33**, 1837–1840.
24 Y. Chu, H. Deng and J.-P. Cheng, *J. Org. Chem.*, 2007, **72**, 7790–7793.
25 M. Hasan, I. V. Kozhevnikov, M. R. H. Siddiqui, A. Steiner and N. Winterton, *Inorg. Chem.*, 1999, **38**, 5637–5641.
26 E. R. Schreiter, J. E. Stevens, M. F. Ortwerth and R. G. Freeman, *Inorg. Chem.*, 1999, **38**, 3935–3937.
27 M. Deetlefs, H. G. Raubenheimer and M. W. Esterhuysen, *Catal. Today*, 2002, **72**, 29–41.
28 F. A. Cotton, G. Wilkinson, C. A. Murillo and M. Bochmann, in *Advanced Inorganic Chemistry*, Wiley-Interscience, 1999, p. 1071.
29 C. J. Serpell, N. L. Kilah, P. J. Costa, V. Félix and P. D. Beer, *Angew. Chem., Int. Ed.*, 2010, **49**, 5322–5326.
30 G. T. Spence, C. J. Serpell, J. Sardinha, P. J. Costa, V. Félix and P. D. Beer, *Chem.–Eur. J.*, 2011, **17**, 12955–12966.
31 C. J. Serpell, J. Cookson, D. Ozkaya and P. D. Beer, *Nat. Chem.*, 2011, **3**, 478–483.
32 H. Nowell, S. A. Barnett, K. E. Christensen, S. J. Teat and D. R. Allan, *J. Synch. Rad.*, 2012, **19**, 435–441.
33 Z. Otwinowski and W. Minor, *Processing of X-ray Diffraction Data Collected in Oscillation Mode*, Academic Press, 1997.
34 CrystalClear-SM Expert 2.0 r4, Rigaku, 2009.
35 G. M. Sheldrick, *Acta Crystallogr., Sect. A: Fundam. Crystallogr.*, 2008, **64**, 600–601.
36 G. C. A. Altomare, C. Giacovazzo, A. Guagliardi, M. C. Burla, G. Polidori and M. Camalli, *J. Appl. Crystallogr.*, 1994, **27**, 435.
37 L. Palatinus and G. Chapuis, *J. Appl. Crystallogr.*, 1997, **40**, 786–790.
38 P. W. Betteridge, J. R. Carruthers, R. I. Cooper, K. Prout and D. J. Watkin, *J. Appl. Crystallogr.*, 2003, **36**, 1487.
39 R. I. Cooper, A. L. Thompson and D. J. Watkin, *J. Appl. Crystallogr.*, 2010, **43**, 1100–1107.
40 A. L. Thompson and D. J. Watkin, *J. Appl. Crystallogr.*, 2011, **44**, 1017–1022.